

Attosecond real-time observation of electron tunnelling in atoms

M. Uiberacker^{1,2}, Th. Uphues³, M. Schultze², A. J. Verhoeef^{2,4}, V. Yakovlev¹, M. F. Kling⁵, J. Rauschenberger^{1,2}, N. M. Kabachnik^{3,6}, H. Schröder², M. Lezius², K. L. Kompa², H.-G. Müller⁵, M. J. J. Vrakking⁵, S. Hendel³, U. Kleineberg¹, U. Heinzmann³, M. Drescher⁷ & F. Krausz^{1,2,4}

Atoms exposed to intense light lose one or more electrons and become ions. In strong fields, the process is predicted to occur via tunnelling through the binding potential that is suppressed by the light field near the peaks of its oscillations. Here we report the real-time observation of this most elementary step in strong-field interactions: light-induced electron tunnelling. The process is found to deplete atomic bound states in sharp steps lasting several hundred attoseconds. This suggests a new technique, attosecond tunnelling, for probing short-lived, transient states of atoms or molecules with high temporal resolution. The utility of attosecond tunnelling is demonstrated by capturing multi-electron excitation (shake-up) and relaxation (cascaded Auger decay) processes with subfemtosecond resolution.

With the invention of the laser in 1960 and subsequent advances in ultrashort light pulse generation, light fields with a strength of several volts per angstrom have become routinely available. They rival the fields acting on valence electrons in atomic systems, allowing their release from atoms, molecules and solids. These advances sparked a revolution in studying the interaction of electrons with light. The primary step in strong-field interactions is the liberation of electrons from their atomic bound state. The revolutionary theory of Keldysh¹ and subsequent work^{2–6} suggested that a valence electron may escape by tunnelling through its atomic binding potential suppressed by the light field (Fig. 1a). If the dimensionless parameter:

$$\gamma = \frac{\omega_L \sqrt{2mW_b}}{|e|E_0} \quad (1)$$

is less than one, under the assumption of $\hbar\omega_L \ll W_b$ ionization is predicted to be confined to short intervals lasting a fraction of the half oscillation cycle of the light field (Fig. 1b). Here E_0 and ω_L stand for the amplitude and angular frequency of the oscillations of the laser electric field $E_L(t) = E_0 \varepsilon(t) \cos(\omega_L t + \varphi)$, with $\varepsilon(t)$ being the amplitude envelope function, and e , m and W_b the charge, mass and binding energy of the electron. Recent studies⁶ suggest that tunnelling remains the dominant ionization mechanism even for γ substantially exceeding one, that is, under conditions when the potential barrier formed by the atomic binding potential and the ionizing light field varies during tunnelling (non-adiabatic regime).

In this work we report what we believe is the first real-time observation of light-induced electron tunnelling. The observation of ionization occurring in subfemtosecond steps spaced by the half laser cycle up to values of the Keldysh parameter as high as three is in good agreement with analytic and numerical calculations. Our approach provides experimental access to all forms of optical field ionization—both adiabatic and nonadiabatic tunnelling, as well as barrier-suppression ionization—and allows us to test models of these processes for the first time.

Once the process of field ionization is fully understood, the technique of attosecond tunnelling will provide direct time-domain

insight into a wide range of multi-electron dynamics and electron–electron interactions, ultimately with a resolution approaching the atomic unit of time (~ 24 as). We demonstrate this potential by probing shake-up and Auger cascade processes with subfemtosecond resolution.

Attosecond probing of electron dynamics

Figure 2 illustrates different options for attosecond sampling of electronic motion in atoms or molecules. A subfemtosecond extreme ultraviolet (XUV) pulse triggers the motion by exciting a valence or core electron (Fig. 2a, b). The unfolding excitation and relaxation processes (Fig. 2) could, in principle, be probed by a delayed replica of the pulse. However, the low flux of currently available subfemtosecond XUV pulses and the low two-photon transition probabilities in the XUV and X-ray regimes have thwarted this straightforward extension of conventional pump–probe techniques into the XUV–X-ray spectral range.

A few-cycle wave of visible or near-infrared (NIR) light with controlled waveform⁷ in combination with a highly nonlinear process may replace the subfemtosecond pulse either in probing or starting electron dynamics. This was first demonstrated by attosecond streaking^{8,9}: the strong-field interaction of a few-cycle light wave with free electrons released by a subfemtosecond XUV excitation pulse results in broadening and shifting of their final momentum distribution. Recording the streaked spectra of the emitted photo- and Auger electrons versus delay between the XUV pump and the few-cycle laser probe allowed us to retrieve the XUV pulse^{10,11} and the laser field¹² as well as the inner-atomic relaxation dynamics¹³ with subfemtosecond resolution.

Here, we demonstrate that nonlinear interaction of the same light wave with bound electrons ionizes in subfemtosecond steps and hence offers a means of probing intra-atomic and intra-molecular electron dynamics—including when no free electrons are released—by means of attosecond tunnelling. This approach relies on the fact that energetic photo-excitation as well as subsequent rearrangement

¹Department für Physik, Ludwig-Maximilians-Universität, Am Coulombwall 1, ²Max-Planck-Institut für Quantenoptik, Hans-Kopfermann-Strasse 1, D-85748 Garching, Germany.

³Fakultät für Physik, Universität Bielefeld, Universitätsstrasse 25, D-33615 Bielefeld, Germany. ⁴Technische Universität Wien, Gusshausstrasse 27, A-1040 Vienna, Austria. ⁵FOM-Instituut voor Atoom- en Molecuulfysica (AMOLF), Kruislaan 407, 1098 SJ, Amsterdam, The Netherlands. ⁶Institute of Nuclear Physics, Moscow State University, Moscow 119992, Russia. ⁷Institut für Experimentalphysik, Universität Hamburg, Luruper Chaussee 149, D-22671 Hamburg, Germany.

via Auger decay is accompanied by transitions to unoccupied orbitals via ‘shake-up’ (Fig. 2d–f)^{14–16}. Here, we use the term ‘shake-up’ in a broad sense, standing for all possible processes populating excited ionic states (including instantaneous and non-instantaneous ones), henceforth referred to as shake-up states (represented by levels 1, 2 and 3 in the example of Fig. 2). These populations can be probed via optical field ionization by a strong, few-cycle NIR pulse of variable delay Δt , with respect to the subfemtosecond XUV excitation (Fig. 1c) by measuring the number of ions resulting from the XUV pump–NIR probe exposure as a function of Δt (Fig. 1d).

Shake-up usually populates several quantum states in the valence band, from which electrons can be freed by the NIR probe. Hence, the ion yield will constitute an integral signal, with contributions from all shake-up states up to a certain binding energy from which ionization is feasible for the intensity chosen. Population dynamics of individual states of significantly differing binding energy can be retrieved by pump–probe scans repeated at different NIR probe intensities and/or from the temporal separation of the depletion of the states in the same delay scan, as explained in Fig. 1d and demonstrated in Fig. 4. The ion yield constitutes an integral signal in a temporal sense, too. The shake-up states are exposed to the ionizing NIR field from the moment they have been populated until the end of the NIR pulse. The

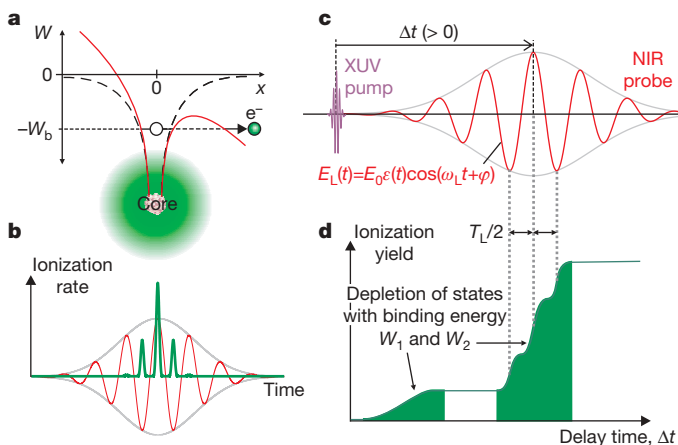


Figure 1 | Strong-field ionization and pump-probe setting for its real-time observation. **a**, Exposing an atom to a strong NIR laser field will result in a modified potential (solid curve) composed of the Coulomb potential (dashed curve) and the time-dependent effective potential of the laser pulse. The laser is polarized along the x direction and W_b is the binding energy of the electron. At sufficiently high laser field strengths the atomic binding potential is suppressed to a small barrier in the x or $-x$ direction for the maxima and minima of the laser electric field, respectively, allowing optical tunnelling to become the dominant ionization mechanism. **b**, The highly nonlinear dependence of the tunnelling rate on the width of the potential barrier confines ionization to time intervals of very short duration near the field oscillation maxima. In the electric field of a few-cycle NIR laser pulse (thin line) ionization is predicted to be restricted to several subfemtosecond intervals (thick line). **c**, Concept for tracing optical-field ionization: a subfemtosecond XUV pulse generates ions in excited (shake-up) states, from which a time-delayed NIR few-cycle probe pulse liberates electrons to produce doubly charged ions. A delay $\Delta t = 0$ is defined as the coincidence of the peaks of the envelopes of the NIR and XUV pulse. $\Delta t > 0$ implies that the peak of the XUV pulse envelope precedes that of the NIR pulse. **d**, Yield of doubly charged ions versus delay Δt between the XUV pump and the NIR probe, as predicted qualitatively for the case of electrons being prepared in two shake-up states of significantly differing binding energy (W_1 and $W_2 \gg W_1$) for liberation via strong-field ionization (see text for discussion). The state of low binding energy is depleted at low intensities, where multiphoton ionization dominates and hence sub-cycle structure in the ionization dynamics is absent. By contrast, the state of high binding energy is emptied by tunnelling, resulting in pronounced sub-half-cycle steps in the ionization profile.

beginning of this time interval within the NIR pulse is adjusted with the delay Δt between the XUV pump and the NIR probe. As the delay is scanned from large negative values (NIR probe first) to large positive values (XUV pump first) the measured ion yield (Fig. 1d) starts increasing at $\Delta t < 0$ owing to ionization on the trailing edge of the NIR pulse and continues to increase with increasing Δt because the XUV pump shifts towards the peak of the ionizing NIR probe and the shake-up states are exposed to ever higher NIR probe intensities.

In the absence of Auger decay, shake-up excitation results from photoionization only (Fig. 2d). The time-dependent ionization dynamics sketched in Fig. 1d can then be traced by measuring the yield of doubly charged ions as a function of the delay between the XUV pump and the sampling NIR light field. The temporal ionization gradients sketched in Fig. 1d incorporate the finite duration of the XUV excitation, a possible delayed response of shake-up and the tunnelling dynamics. With a sufficiently rapid ($\ll 1$ fs) excitation, these measurements can thus provide direct insight into the temporal evolution of shake-up (in the presence of a strong optical field) and light-induced tunnelling. In what follows, first we prove this concept by exposing neon atoms to our subfemtosecond XUV pump and few-cycle NIR probe pulses (Fig. 3) and measuring the yield of the product of the pump–probe exposure, Ne^{2+} , versus Δt (Fig. 4). Then we extend the approach to probing electrons shaken up in xenon atoms during Auger decay. Our primary observables in this case are higher charged states, Xe^{N+} (for $N > 2$). Measuring their yield versus Δt displays the course of an Auger cascade.

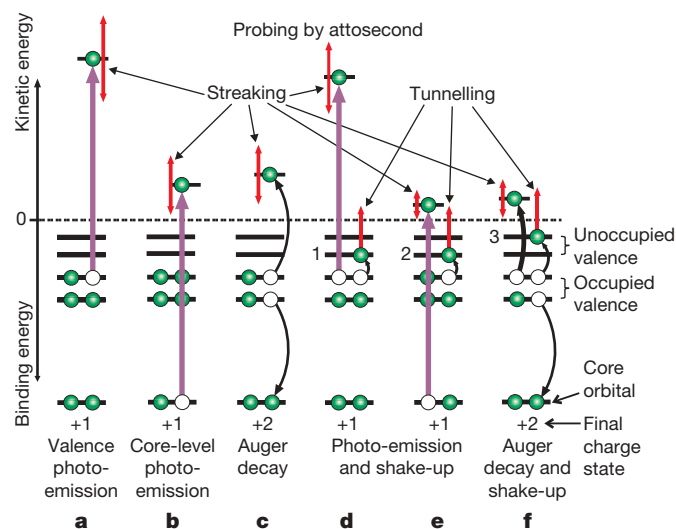


Figure 2 | Probing electron dynamics in atoms, molecules or solids with attosecond sampling techniques. A subfemtosecond XUV pulse triggers the motion by inducing valence (process **a**) or core photoelectron emission (process **b**). The temporal evolution of photo- and Auger electron emission (process **c**) can be probed via attosecond streaking to retrieve the XUV pump pulse or the sampling NIR field and trace inner-shell relaxation dynamics. XUV photoexcitation as well as subsequent Auger decay processes are usually accompanied by shake-up of another electron to a previously unoccupied level (processes **d**, **e** and **f**). In this case the liberated electrons will be ejected at a reduced kinetic energy compared to the cases without shake-up processes **a**, **b** and **c**. The difference in energy is used for shaking up bound electrons (represented by curved black arrows to levels 1, 2 and 3). For sufficiently strong probing laser fields, the shake-up electrons can be liberated by tunnelling ionization. The temporal evolution of the tunnelling current will provide information about the inner-atomic electron dynamics that populates and/or depopulates the interrogated shake-up states and the duration of the process that have populated the levels on atto- and femtosecond timescales. Note that the final charge state given in the figure is increased by attosecond tunnelling, while it remains unchanged in the case of attosecond streaking. The observable for streaking is the momentum distribution of liberated electrons, whereas in tunnelling it is the number of ions in different charge states.

Experimental set-up

For a detailed description of the attosecond pump–probe apparatus, see the Supplementary Information. Briefly, the XUV pump originates from high-harmonic generation in a neon gas jet exposed to 300- μ J, 750-nm waveform-controlled laser pulses with a duration of $\tau_L \approx (5.5 \pm 0.5)$ fs, at a repetition rate of 3 kHz. The collinear, linearly polarized XUV and NIR light beams are passed through several filters and reflected by a concentric double-mirror arrangement (Mo/Si multilayer: ~ 9 eV bandwidth at photon energy of 91 eV). The mirror introduces a variable delay between the XUV and the NIR fields, isolates a single or twin XUV pulse (depending on the carrier-envelope phase of the laser pulse) of $\tau_X \approx 250$ as duration¹¹ by filtering the cut-off part of the harmonic emission spectrum and focuses both beams into a jet of atoms under scrutiny. The absolute delay between the XUV and the NIR signals is determined with an accuracy of better than ± 0.5 fs; for details see Supplementary Information. Ions created in the common focus of the two beams are detected by a time-of-flight ion spectrometer (reflectron) that combines high mass resolution ($\Delta m/m \approx 10^{-3}$) with the capability of analysing

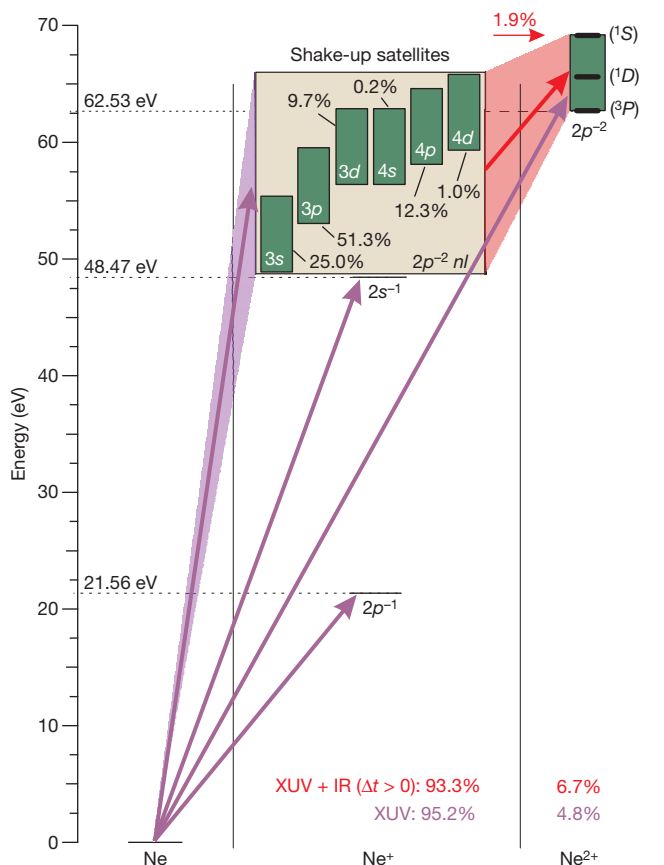


Figure 3 | Energy levels and transitions in Ne^{1+} and Ne^{2+} ions relevant to this study. The plotted levels represent energies required to ionize and possibly excite a neutral atom from its ground state. Absorption of photons of about 91-eV energy can produce singly or doubly charged ions with probabilities of 95.2% and 4.8%, respectively. Owing to shake-up a small fraction of the singly-charged ions is produced in $2p^{-2}nl$ configurations, where the probabilities of different channels are known from electron spectroscopy (see Supplementary Information). Each of these configurations, represented by a green box, consists of $2p^{-2}(^3P)nl$, $2p^{-2}(^1D)nl$, and $2p^{-2}(^1S)nl$ states (the atomic terms in parentheses describe electrons not involved in the interaction). Our few-cycle laser field following the XUV pulse ($\Delta t > 0$) can remove electrons from these shake-up states, thus increasing the probability of double ionization to 6.7%. Depending on the initial $2p^{-2}nl$ state, the doubly ionized ion is left in one of the 3P , 1D or 1S states. On its own, the laser pulse produces only singly charged ions (in configuration $2p^{-1}$) above the detection limit.

particles within a micrometre-scale detection volume^{17–19}. The target and background pressures were $\sim 10^{-2}$ and $\sim 10^{-8}$ mbar, respectively.

Shake-up and tunnelling

To probe shake-up and light-induced electron tunneling, we ionized neon atoms with our subfemtosecond XUV pulse. Figure 3 shows the level structure and transitions relevant to our experiments. The core shell was not accessed by our XUV photons, and hence Auger decay is absent²⁰. The threshold energies for single and double ionization from the outer shell of Ne are 21.56 and 62.53 eV, respectively²¹. The XUV photons produced Ne^{1+} and Ne^{2+} ions with a ratio of

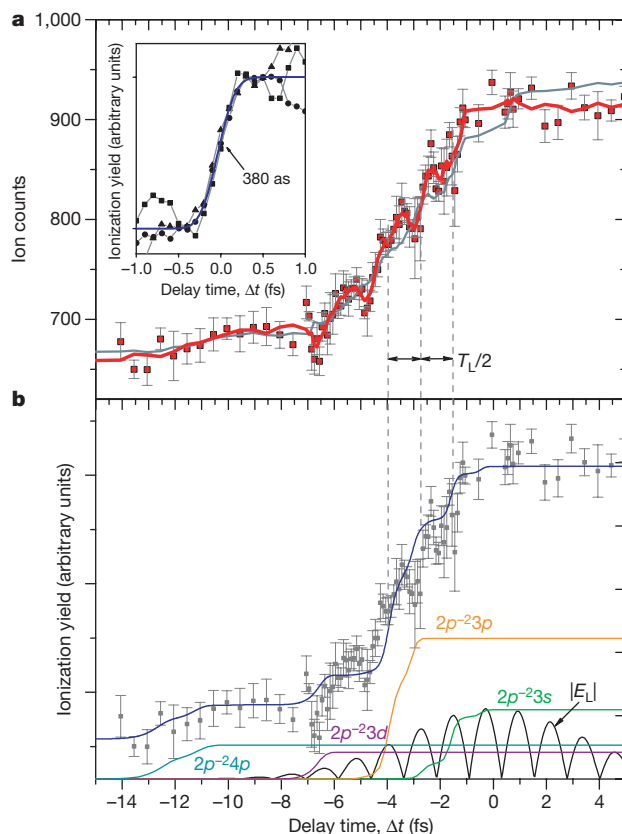


Figure 4 | Ne^{2+} ion yield versus delay between the subfemtosecond XUV pump and the few-cycle NIR probe: experiment and modelling. The peak intensity of the NIR probe was $(7 \pm 1) \times 10^{13} \text{ W cm}^{-2}$. **a**, The experimental data were acquired from six delay scans repeated under the same experimental conditions. The signal was accumulated for 3 s at each delay setting. The squares and error bars show the average and the standard error (s.e.m.) of the results of the six measurements. The thick red line shows the average of five adjacent data points; the thin grey line shows the same as the thick line but recorded with NIR probe pulses of random carrier-envelope phase. In the inset, squares, triangles, and circles depict an ionization step extracted from three different measurements normalized to give the same change in the ionization yield. The solid line shows an error-function fit to the data yielding a rise time of 380 as (full-width at half-maximum, FWHM, of the gaussian function derived from the error function). The zero of delay is set arbitrarily to the centre of the tunnelling process. **b**, Simulation of the pump–probe experiment based on the nonadiabatic theory of tunnel ionization⁶. The thin coloured lines show the calculated fractional ionization yields contributed by electrons liberated from different shake-up states. The thick blue line depicts the overall ionization rate obtained by totalling the fractional rates (and by adding the result to the background measured at large negative delays). The simulations were carried out for a gaussian 250-as XUV pulse and a gaussian 5.5-fs laser pulse with a peak intensity of $7 \times 10^{13} \text{ W cm}^{-2}$. The black solid curve represents the absolute value of the laser field. For discussion of the results, see text.

(19.7 ± 0.5):1 (with $\sim 2,500 \text{ Ne}^{1+}$ ions created per second), in good agreement with the results of synchrotron measurements²². A few per cent of the Ne^{1+} ions were promoted into $2p^{-2}nl$ (principal quantum number n : 3 or 4; quantum orbit l : s , p or d) configurations²³ (Fig. 3). These satellite states can only decay radiatively on a picosecond time-scale.

Double ionization by the NIR field was not observed at the intensity level chosen. The XUV-generated Ne^{2+} yield was therefore not affected by the NIR probe for $\Delta t \ll -\tau_L$ but was significantly enhanced by the laser field for Δt approaching zero and becoming positive. The NIR-induced Ne^{2+} yield enhancement amounted to $(40 \pm 4)\%$ of the XUV-produced Ne^{2+} yield at a NIR peak intensity of $(7 \pm 1) \times 10^{13} \text{ W cm}^{-2}$. The absence of this enhancement for $\Delta t \ll -\tau_L$ clearly indicates that the laser sets electrons free from states excited by the XUV pulse as sketched in Fig. 2d. The laser-induced change in the Ne^{2+} yield amounts to some 2% of the XUV-produced Ne^{1+} ions. This implies that a substantial fraction of the population of the $2p^{-2}nl$ shake-up satellites must have been depleted by field ionization.

Figure 4a shows the number of Ne^{2+} ions detected as a function of delay Δt between the XUV pump and NIR probe. Figure 4b compares the prediction of the Yudin–Ivanov theory⁶ (lines) with the experimental data (squares). In our modelling the shake-up states were populated instantly during XUV photoionization (for more details, see Supplementary Information). The calculations are in reasonable agreement with our measurements and reveal how the different shake-up states are depleted sequentially by laser-field ionization. The signal starts increasing at large negative delays owing to depletion of the $2p^{-2}4p$ state (relative population $\sim 12\%$) and the $2p^{-2}3d$ state ($\sim 10\%$) at NIR intensity levels reached some 10 and 6 fs after the peak of the NIR probe ($\Delta t \sim -10$ and -6 fs), respectively. A more dramatic increase in the Ne^{2+} yield is observed as the delay approaches zero, as a consequence of the depletion of the most highly populated $2p^{-2}3p$ ($\sim 50\%$) and $2p^{-2}3s$ ($\sim 25\%$) states. In spite of their relatively high binding energy (~ 10 and 13 eV, respectively), these states are also depleted before zero delay, that is, by the field oscillation cycles comprised in the trailing edge of the pulse, leaving no room for increasing the Ne^{2+} yield with increasing Δt beyond 0. This main contribution to the Ne^{2+} yield emerges within approximately one and a half wave cycles of the NIR field, $\sim (3/2)T_L = 3\pi/\omega_L$, in several sharp steps that are spaced by $\sim T_L/2$; this clearly shows that field-induced tunnelling is the main cause of the observed increase in the Ne^{2+} yield. This conclusion is also supported by the disappearance of the steps in a pump–probe scan performed with a randomly varying carrier-envelope phase of the NIR probe pulses (grey line in Fig. 4a).

The main shake-up population (residing in the $2p^{-2}3p$ and $2p^{-2}3s$ states) is depleted at NIR intensities corresponding to a Keldysh parameter γ of the order of three. Hence, our experiment verifies not only the existence of light-field-induced tunnelling, as predicted by Keldysh some four decades ago¹, but also confirms the dominant role of this ionization mechanism up to γ values substantially exceeding 1, as predicted recently by Yudin and Ivanov⁶. This conclusion is also backed by numerical solutions of the time-dependent Schrödinger equation (see Supplementary Information).

The steepness of the ionization steps and the dips preceding them in the measured data are not well reproduced by our model, which neglects the influence of electron–electron interactions and that of the strong NIR field on the XUV-induced transitions populating the shake-up states. Recent work²⁴ and our TDSE simulations (see Supplementary Information) indicate that the influence of the strong laser field on the XUV excitation process may (at least partially) be responsible for this discrepancy.

We feel that these experiments afford profound insight into fundamental electronic processes such as tunnelling and shake-up by contrasting theoretical models with time-domain data. To exploit this potential both (1) accurate models of shake-up in the presence

of a strong laser field need to be developed and (2) the temporal resolution needs to be improved by using shorter XUV pulses²⁵ and improving the signal-to-noise ratio as well as the accuracy of determining the zero of delay. These advances will allow determination of the attosecond temporal evolution of the light-field-induced tunnelling current and they will provide deep insight into the nature of the electron–electron interactions responsible for shake-up.

Once models for shake-up and tunnelling have been tested and verified with attosecond precision, the technique of attosecond tunnelling will provide direct time-domain insight into a wide range of multi-electron dynamics inside atoms and molecules by probing the transient population of excited valence states while these dynamics are unfolding. With improved signal-to-noise and XUV pulse duration, the temporal resolution may potentially approach the atomic unit of time (~ 24 as). At present, the observed rise time of the Ne^{2+} yield of less than 400 as (which sets a corresponding upper limit on the time it takes the excited electronic states to become populated during XUV ionization and on tunnelling; see inset in Fig. 4a) dictates the temporal resolution of our pump–probe approach. In the next section we demonstrate its applicability to probing intra-atomic multi-electron dynamics in real time.

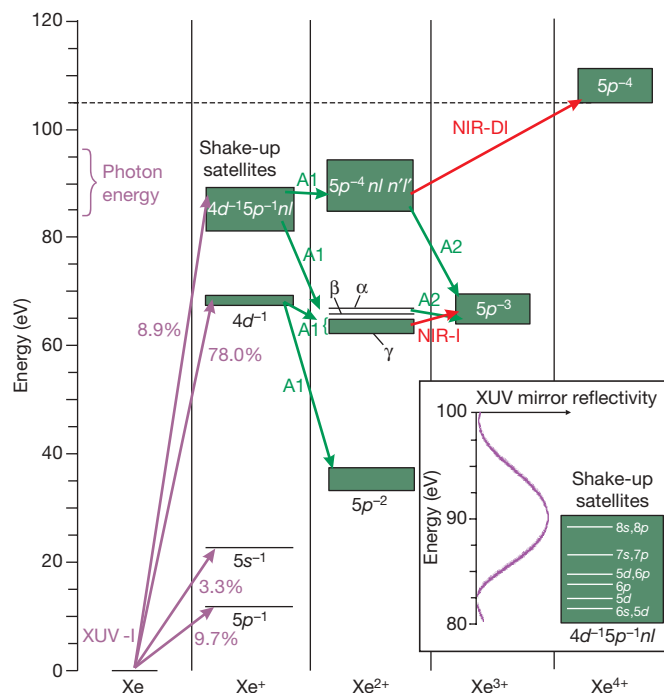


Figure 5 | Energy levels and transitions in xenon ions relevant to the current study. The relative population of states in Xe^{1+} is given for an XUV excitation energy of 90 eV from ref. 30. The XUV light preferably ionizes from the $4d^{-1}$ shell, creating an inner-shell vacancy. A subsequent Auger process (green arrows labelled A1) will follow with 99% probability²⁶ and is predominantly decaying to Xe^{2+} in configuration $5p^{-2}$. Some of the populated states, α and β (presumably $5s^{-1}5p^{-2}7p$ states^{28,31}) can further decay to Xe^{3+} via a second Auger process (green arrow labelled A2), leading to triply charged ions. The A1 process also populates states below the threshold for Xe^{3+} . These are denoted by γ and represent $5s^{-1}5p^{-2}6p$ as well as $5p^{-2}nl$ configurations. The laser pulse can ionize these states (red arrow labelled NIR-I). Furthermore, a series of $4d^{-1}$ shake-up satellites in Xe^{1+} is also populated—with a small probability—by the XUV pulse. The inset shows the possible configurations²⁹ together with the XUV mirror reflectivity determining the XUV excitation spectrum. The satellites mainly decay to the α , β , γ states, with a small fraction of the Xe^{2+} population ending up in $5p^{-4}nl n'l'$ configurations. These states are short-lived and decay via the A2 process. Before this occurs, the $nl n'l'$ electrons can be liberated by the laser field to yield Xe^{4+} in the $5p^{-4}$ state (red arrow labelled NIR-DI).

Multi-electron relaxation

As a first application of the technique of attosecond tunnelling, we captured Auger cascade xenon atoms following excitation by a sub-femtosecond XUV pulse. Figure 5 sketches the relevant energy levels and transitions. Energy-resolved synchrotron measurements have revealed that (1) the 91-eV XUV pulse will preferably liberate electrons from the $4d$ orbital²², (2) the vacancy decays by subsequent single (A1 in Fig. 5) and cascaded (A1 and A2 in Fig. 5) Auger processes, leading to Xe^{2+} and Xe^{3+} , respectively²⁶, and (3) the lifetimes of the $4d_{3/2}$ and $4d_{5/2}$ holes are 6.3 ± 0.2 and 5.9 ± 0.2 fs, respectively²⁷. These time-integral measurements have hitherto been able to set only a lower limit of 23 fs for the time constant of A2 (ref. 27).

To trace this dynamics in real time, we simultaneously recorded the number of Xe ions emerging in different charged states as a function of Δt . At the laser intensity of $(7 \pm 1) \times 10^{13} \text{ W cm}^{-2}$ used in this experiment, the XUV-induced Xe^{1+} yield is buried in laser-generated background, preventing delay-dependent effects from coming to light in the Xe^{1+} signal. This is not the case for higher charged states. With increasing delay, rapid exponential increase was observed in the Xe^{3+} signal near $\Delta t = 0$ (Fig. 6b), concurrent with a significant decrease of the Xe^{2+} yield. The background in the Xe^{3+} signal arises from the A1–A2 Auger cascade discussed above. From

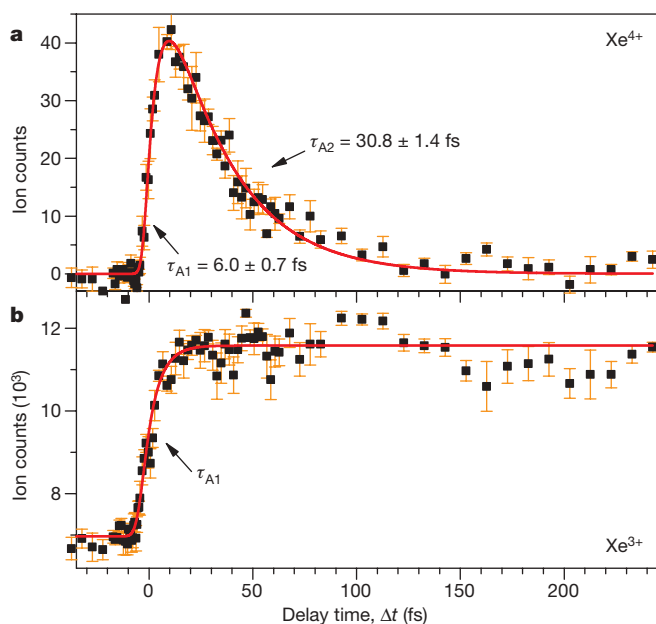


Figure 6 | Xe^{4+} and Xe^{3+} ion yields versus delay between the subfemtosecond XUV pump and the few-cycle NIR probe. The data have been compiled from the results of five delay scans repeated under the same experimental conditions. The signals were accumulated for 20 s at each delay setting. The squares and the error bars show the average and the s.e.m. of the results of these measurements. **a**, Assuming a sampling function identical to the ionization profile measured in the neon experiment (see solid line in Fig. 4a), a double exponential fit (see Supplementary Information) to the measured Xe^{4+} yield versus Δt (solid line) yields the Auger decay times $\tau_{A1} = 6.0 \pm 0.7$ fs and $\tau_{A2} = 30.8 \pm 1.4$ fs. **b**, With the temporal evolution of the A1 process acquired from the Xe^{4+} data and using the fact that the rise of the Xe^{3+} yield with τ comprises both A1 and the laser-induced ionization process, we can obtain the temporal evolution of the laser-induced transition from that of the Xe^{3+} yield. The exponential rise from about 7,000 to 11,500 counts is consistent with a laser-induced ionization time of 5.8 ± 2.5 fs (FWHM). This is comparable to τ_L , indicating that low-order, one-photon and/or two-photon transitions may promote electrons from the γ states of Xe^{2+} to the $5p^{-3}$ states of Xe^{3+} (see Fig. 5). Note that the fluctuations in the Xe^{3+} signal can be largely accounted for by XUV intensity variations, which can be efficiently eliminated by normalization to, for example, the Xe^{2+} ion yield (see Supplementary Information).

Fig. 5 we infer that the laser-induced increase in the Xe^{3+} yield is due to ionization from the γ -states in Xe^{2+} , which cannot spontaneously decay into Xe^{3+} . This NIR-probe-induced transition (denoted by NIR-I in Fig. 5) yields Xe^{3+} in configuration $5p^{-3}$. Because these are populated by the first Auger process, A1, the exponential increase in the Xe^{3+} signal is the convolution of the A1 decay and the NIR-induced ionization process. No decrease of the enhanced Xe^{3+} yield was observed up to our maximum delay of 300 fs, indicating that the lifetime of the γ states was longer than 1 ps.

Charge-states higher than Xe^{3+} cannot be created with the XUV pulse alone, because the XUV photon energy is below the threshold for Xe^{4+} production (~ 105 eV). However, with the probe switched on, we did observe Xe^{4+} ions for $\Delta t > -\tau_L$ (Fig. 6a). The Xe^{4+} signal first grows within a few femtoseconds, followed by a longer decay. The Xe^{4+} ions are created by NIR-induced double ionization (denoted by NIR-DI in Fig. 5) from the intermediate doubly excited $5p^{-4}nl'n'l'$ (Fig. 5) and/or singly excited $5s^{-2}5p^{-1}nl$ (not shown in Fig. 5) states of Xe^{2+} . These states are populated by A1 from the satellites $4d^{-1}5p^{-1}nl$ of the $4d^{-1}$ state upon emission of low-energy electrons^{28,29} and emptied by A2 to states of larger binding energy in Xe^{3+} , which cannot be reached by the NIR probe.

From these results we conclude that the exponential rise and decay of the Xe^{4+} signal in Fig. 6a reveal the evolution of the A1 and A2 Auger decays, respectively. The laser-induced double ionization may be either sequential or non-sequential (with the second step induced by recollision of the first electron). In either case, in the first step a binding energy similar to that of the most highly populated shake-up states in the neon experiment must be overcome by tunnel ionization. Hence, the probing (ionization) process may be assumed to be the same as measured in the neon experiment, see Fig. 4a. With this sampling function, fitting the result of a simple rate-equation analysis including the transitions A1 and A2 to the Xe^{4+} data shown in Fig. 6 yields decay times of $\tau_{A1} = 6.0 \pm 0.7$ fs and $\tau_{A2} = 30.8 \pm 1.4$ fs for the A1 and A2 Auger processes, respectively. Both time constants are in accordance with the results of energy-resolved measurements²⁷.

Conclusions and outlook

We have reported the observation of light-induced electron tunnelling from atoms in real time. Electrons are found to escape from their atomic binding potential within several subfemtosecond time intervals near the oscillation peaks of the ionizing few-cycle near-infrared laser field. Our results are in good agreement with the predictions of the theory Keldysh put forward four decades ago. The observed subfemtosecond ionization steps provide a powerful means of probing the transient population of short-lived valence electronic states in excited atoms or molecules, offering direct, time-domain access to a wide range of multi-electron dynamics unfolding on an attosecond to femtosecond timescale. Proof-of-principle attosecond tunnelling experiments in neon and xenon demonstrate this potential. Simultaneous implementation of attosecond tunnelling and attosecond streaking spectroscopy along with scaling of the techniques to higher photon energies and shorter X-ray pulse durations will provide unprecedented insight into the transient electronic states of matter.

Received 2 November 2006; accepted 26 January 2007.

1. Keldysh, L. V. Ionization in the field of a strong electromagnetic wave. *Sov. Phys. JETP* **20**, 1307–1314 (1965).
2. Faisal, F. H. M. Multiple absorption of laser photons by atoms. *J. Phys. B* **6**, L89–L92 (1973).
3. Reiss, H. R. Effect of an intense electromagnetic field on a weakly bound system. *Phys. Rev. A* **22**, 1786–1813 (1980).
4. Brabec, T. & Krausz, F. Intense few-cycle laser fields: frontiers of nonlinear optics. *Rev. Mod. Phys.* **72**, 545–591 (2000).
5. Scrinzi, A., Geissler, M. & Brabec, T. Ionization above the coulomb barrier. *Phys. Rev. Lett.* **83**, 706–709 (1999).
6. Yudin, G. L. & Ivanov, M. Yu. Nonadiabatic tunnel ionization: looking inside a laser cycle. *Phys. Rev. A* **64**, 013409 (2001).

7. Baltuska, A. *et al.* Attosecond control of electronic processes by intense light fields. *Nature* **421**, 611–615 (2003).
8. Itatani, J. *et al.* Attosecond streak camera. *Phys. Rev. Lett.* **88**, 173903 (2002).
9. Kitzler, M., Milosevic, N., Scrinzi, A., Krausz, F. & Brabec, T. Quantum theory of attosecond XUV pulse measurement by laser-dressed photoionization. *Phys. Rev. Lett.* **88**, 173904 (2002).
10. Hentschel, M. *et al.* Attosecond metrology. *Nature* **414**, 509–513 (2001).
11. Kienberger, R. *et al.* Atomic transient recorder. *Nature* **427**, 817–821 (2004).
12. Goulielmakis, E. *et al.* Direct measurement of light waves. *Science* **305**, 1267–1269 (2004).
13. Drescher, M. *et al.* Time-resolved atomic inner-shell spectroscopy. *Nature* **419**, 783–787 (2002).
14. Svensson, S., Eriksson, B., Martensson, N., Wendin, G. & Gelius, U. Electron shake-up and correlation satellites and continuum shake-off distributions in x-ray photoelectron spectra of the rare gas atoms. *J. Electron Spectrosc. Related Phenomena* **47**, 327–384 (1988).
15. Aksela, H., Aksela, S. & Kabachnik, N. Resonant and nonresonant Auger recombination. In *VUV and Soft X-Ray Photoionization* (eds Becker, U. & Shirley, D. A.) 401–440 (Plenum, New York, 1996).
16. Istomin, A. Y., Manakov, N. L. & Starace, A. F. Perturbative analysis of the triply differential cross section and circular dichroism in photo-double-ionization of He. *Phys. Rev. A* **69**, 032713 (2004).
17. Schröder, H., Wagner, M., Kaesdorf, S. & Kompa, K. L. Surface-analysis by laser ionization. *Ber. Bunsenges. Phys. Chem.* **97**, 1688–1692 (1993).
18. Wagner, M. & Schröder, H. A novel 4 grid ion reflector for saturation of laser multiphoton ionization yields in a time-of-flight mass-spectrometer. *Int. J. Mass Spectrom.* **128**, 31–45 (1993).
19. Witzel, B., Schröder, H., Kaesdorf, S. & Kompa, K. L. Exact determination of spatially resolved ion concentrations in focused laser beams. *Int. J. Mass Spectrom.* **172**, 229–238 (1998).
20. Larkins, F. P. Charge state dependence of x-ray and Auger electron emission spectra for rare-gas atoms—II. The neon atom. *J. Phys. B* **4**, 14–19 (1971).
21. National Institute of Standards and Technology *Physical Reference Data* (<http://physics.nist.gov/PhysRefData/>) (1994).
22. Holland, D. M. P., Codling, K., West, J. B. & Marr, G. V. Multiple photoionization in the rare gases from threshold to 280 eV. *J. Phys. B* **12**, 2465–2484 (1979).
23. Becker, U. & Shirley, D. A. Partial Cross Sections and Angular Distributions. In *VUV and Soft X-Ray Photoionization* (eds Becker, U. & Shirley, D. A.) 135–173 (Plenum, New York, 1996).
24. Smirnova, O., Spanner, M. & Ivanov, M. Y. Coulomb and polarization effects in laser-assisted XUV ionization. *J. Phys. B* **39**, 323–339 (2006).
25. Sansone, G. *et al.* Isolated single-cycle attosecond pulses. *Science* **314**, 443–446 (2006).
26. Kämmerling, B., Krässig, B. & Schmidt, V. Direct measurement for the decay probabilities of 4d_j hole states in xenon by means of photoelectron-ion coincidences. *J. Phys. B* **25**, 3621–3629 (1992).
27. Penent, F., Palaudoux, J., Lablanquie, P. & Andric, L. Multielectron spectroscopy: the xenon 4d hole double Auger decay. *Phys. Rev. Lett.* **95**, 083002 (2005).
28. Lablanquie, P. *et al.* Photoemission of threshold electrons in the vicinity of the xenon 4d hole: dynamics of Auger decay. *J. Phys. B* **35**, 3265–3295 (2002).
29. Hayaishi, T. *et al.* Manifestation of Kr 3d and Xe 4d conjugate shake-up satellites in threshold-electron spectra. *Phys. Rev. A* **44**, R2771–R2774 (1991).
30. Becker, U. *et al.* Subshell photoionization of Xe between 40 and 1000 eV. *Phys. Rev. A* **39**, 3902–3911 (1989).
31. Viehhaus, J. *et al.* Auger cascades versus direct double Auger: relaxation processes following photoionization of the Kr 3d and Xe 4d, 3d inner shells. *J. Phys. B* **38**, 3885–3903 (2005).

Supplementary Information is linked to the online version of the paper at www.nature.com/nature.

Acknowledgements We thank A. F. Starace for discussions. We are grateful for financial support from the Volkswagenstiftung (Germany), the Marie Curie Research Training Network XTRA, Laserlab Europe, and a Marie Curie Intra-European Fellowship. F.K. acknowledges support from the FWF (Austria). The research of M.F.K. and M.J.J.V. is part of the research programme of the Stichting voor Fundamenteel Onderzoek der Materie, which is financially supported by the Nederlandse Organisatie voor Wetenschappelijk Onderzoek. This research was supported by the cluster of excellence Munich Centre for Advanced Photonics (www.munich-photonics.de).

Author Contributions M.U., Th.U., M.S. and A.J.V. contributed equally to this work.

Author Information Reprints and permissions information is available at www.nature.com/reprints. The authors declare no competing financial interests. Correspondence and requests for materials should be addressed to M.U. (matthias.uiberacker@mpq.mpg.de) or F.K. (ferenc.krausz@mpq.mpg.de).